Blockage of STAT3 during epileptogenesis prevents GABAergic loss and imprinting of the epileptic state

Soraya Martín-Suárez,[1,†] Jesús María Cortes[1,2,3] and Paolo Bonifazi[1,2]

Abstract

Epilepsy, the condition of recurrent unprovoked seizures resulting from a wide variety of causes, is one of the world's most prominent neurological disabilities. Seizures which are an expression of neuronal network dysfunction occur in a positive feedback loop of concomitant factors, including also neuro-inflammatory responses, where seizures generate more seizures. Among other pathways involved in inflammatory responses, the JAK/STAT signaling pathway has been proposed to participate in epilepsy. We tested here an in vitro-model of temporal lobe epilepsy, the hypothesis that acute blockage of STAT3-phosphorylation during epileptogenesis, would prevent structural damages in the hippocampal circuitry, and the imprinting of both neural epileptic activity and inflammatory glial states. We performed calcium imaging of spontaneous circuits' dynamics in organotypic hippocampal slices previously exposed to epileptogenic conditions through the blockage of GABAergic synaptic transmission. Epileptogenic conditions lead to epileptic dynamics imprinted on circuits in terms of increased neuronal firing and circuit synchronization, increased correlated activity in neuronal pairs and decreased complexity in synchronization patterns. Acute blockage of the STAT3-phosphorylation during epileptogenesis prevented the imprinting of epileptic activity patterns, general cell loss, loss of GABAergic neurons and the persistence of reactive glial states. This work provides mechanistic evidence that blocking the STAT3 signaling pathway during epileptogenesis can prevent patho-topological persistent reorganization of neuro-glial circuits.

Author affiliations:

1 Computational Neuroimaging Lab, Biocruces-Bizkaia Health Research Institute, 48903 Barakaldo, Bizkaia, Spain

2 IKERBASQUE: The Basque Foundation for Science, 48009, Bilbao, Spain.

3 Department of Cell Biology and Histology, University of the Basque Country (UPV/EHU), Barrio Sarriena s/n, 48940 Leioa, Spain

†Present address: Achucarro Basque Center for Neuroscience. Edificio Sede 3p. Barrio Sarriena s/n, 48940 Leioa, Spain

Correspondence to: Paolo Bonifazi

Computational Neuroimaging Lab, Biocruces-Bizkaia Health Research Institute, Barakaldo. Cruces Plaza, 48903 Barakaldo, Bizkaia, Spain

E-mail: paol.bonifazi@gmail.com

Correspondence may also be addressed to: Soraya Martín-Suárez

Laboratory of Neural Stem Cells and Neurogenesis; Science Park of the UPV/EHU. Sede Building, 3rd floor, Barrio Sarriena, s/n, E-48940 Leioa Spain

E-mail: soraya.martin@achucarro.org

Running title: Blockage of STAT3 prevents the epileptic state

Keywords: Calcium imaging; epilepsy; STAT3; gliosis; GABA

Abbreviations: CNT= Control; CNT WP= Control + WP1066; CNQX= 6-Cyano-7-nitroquinoxaline-2,3-dione,; D-AP5= D-2-amino-5-phosphonopentanoate; DIV= Days In vitro; GCL= granular cell layer region; GFAP= Glial fibrillary acidic protein; GSI= global synchronization index at time t; IF= Instantaneous firing rate; KS-S= Kolmogorov-Smirnov statistics; NS= Network synchronizations; PTX= Picrotoxin; PTX WP= Picrotoxin + WP1066; SGZ= Subgranular zone; STAT3= Signal transducer and activator of transcription 3; TLE=Temporal Lobe epilepsy

Introduction

Epilepsy is a neurological disorder characterized by chronic aberrant patterns of cerebral activity, i.e. seizures, which display in conjunction with other symptoms such as convulsions, loss of consciousness, mental absence and others. Typically, once appeared, epileptic patterns remain imprinted in the brain, and ictal activity re-display chronically, possibly developing and scaling up symptoms with additional dysfunctional problems [1–4]. The relation between causes, prognosis and symptomatology is broad, complex and not fully understood [5]. As a result, not all epileptic patients respond equally to the same drugs [6,7]. Anti-epileptic drugs can work through different mechanisms and often are aimed at preventing hyper-excitable brain conditions which are the fertile substrate for ictal patterns to appear and uncontrollably spread to the rest of the brain [8,9].

The epileptogenic process leading to the final imprinting of an epileptic brain has been hypothesized to be a positive feedback loop where seizures lead to more seizures through complex interactions which involve, among others, neuronal death, gliosis, emergence of aberrant connectivity, hyperexcitation, and neuroinflammation [10]. In the case of temporal lobe epilepsy (TLE), the most prevalent form of epilepsy, the circuit originating the seizures is located in the temporal region of the brain, specifically in the hippocampus. Although the causes that make the hippocampus epileptogenic are not always necessarily known, and drugs are not always effective as treatment, sometimes its surgical removal can lead to the disappearance of the seizures, confirming its key role in the generation of ictal activity [11].

Understanding the mechanisms underlying epileptogenesis, i.e. what turns a functional circuit into an epileptic one capable to generate ictal patterns of activity, is still a major open question, the key for developing new effective treatments for epilepsy.

In our study, we aimed to provide a clearer link between gliosis (an initial marker of neuro-glial inflammatory response) and epileptogenesis. In the last years clinical studies and experimental finding confirmed that the inflammatory pathways are implicated in the epilepsy. Although several signalling pathways have been suggested to participate in the development and progression of epilepsy, here we focused on the JAK/STAT signalling pathway, and in particular, on the STAT3 transcription factor. This pathway is involved in multiple processes such as cellular proliferation, differentiation, neuron survival, death, and synaptic plasticity[12–14]. Induction of epilepsy leads to

activation of STAT3 [15] therefore it has been hypothesized that its inhibition could reduce the neuronal damage and the progression of the epilepsy. The inhibitor of the STAT3 pathway, WP1066, has been reported to reduce the seizure severity and the progression of early epileptogenesis in a mouse model of epilepsy [16] but the mechanisms of such effect are far of being understood.

In our study, we hypothesized that the acute blockage of STAT3 in presence of pro-epileptic conditions, could attenuate the damage induced by the reactive gliosis response on the brain circuits preventing the manifestation of epileptic activity [16] , and cell loss.

Our results lie in the longitudinal monitoring of the activity of circuits previously exposed to epileptogenic hyperexcitation, by simultaneous blockage of GABAergic synaptic transmission and STAT3 signalling. In particular we show that impacting the JAK/STAT pathway prevent the future appearance of hyper-synchronized patterns of activity, cell loss, depletion of inhibitory cells and persistence of gliosis (a main marker for neuro-glial inflammatory states). Our study provides strong support that acute treatments impacting reactive gliosis can prevent patho-topological reorganizations that lead to the imprinting of epileptic dynamics.

Materials and methods

Hippocampal Organotypic Slice Cultures

Slice cultures preparation was done as described in[17]. In brief, P5-7 Wild type pups were decapitated and the brains extracted and placed in cold dissection medium (96% HBSS, 2% HEPES, 1% penicillin/streptomycin, 0.7% glucose (2.5M) and 0.3% of NaOH (0.5 M). Both hippocampi were dissected out and cut into 300µm slices using a vibratome. Both hippocampi were cut in cold artificial CSF (195mM Sucrose; 2.5 mM KCl; 1.25mM NaH_2PO_4; 28mM $NaHCO_3$; 0.5mM $CaCl_2$; 1 mM L-Ascorbic Acid/Na-Ascorbate; 3mM Pyruvic Acid/Na-Pyruvate; 7mM Glucose; 7mM $MgCl_2$ in MiliQ), bubbled with 5% CO_2 [18]. After slicing slices were then transferred to 0.4 µm culture plate inserts (Millipore, PICM01250). The membranes were placed in 24-well plates, each well containing 250µl of culture medium. The medium consisted of 50% Minimum Essential Medium supplemented with 2% B27, 25% horse serum, 2% Glutamax, 0,5% penicillin/streptomycin, 0.5% of NaHCO3, 0,5% glucose(2,5M), 0,8% sucrose (2.5M) and 18%

HBSS. Slices were incubated at 37°C and 5% CO_2 changing media the first day after doing the culture and every 2 days afterwards. Slices were kept in culture for 7 days before change to fresh culturing medium without B27 [18,19].

Epilepsy was induced by the addition of the $GABA_A$ receptor inhibitor picrotoxin (PTX; 100 µM). PTX, vehicle or the inhibitor of Stat3 pathway, WP1066 (1.25 µM) was added with serum-free media for 3 days (just in the case of the results shown in supp fig. 1 A-B and supp. Fig 2 A-B it was added for 1 day starting at 12 days in-vitro). During the induction of epilepsy the medium was replaced every day adding fresh serum-free media and PTX/vehicle and/or WP1066.

To evaluate the role of glutamatergic synaptic transmission on induced circuits' dynamics following epileptogenic conditions (i.e. 3 days after exposure to PTX), we blocked simultaneously AMPA/kainate and NMDA receptors applying respectively CNQX (20µM) and D-AP5 (10µM).

Calcium Imaging Set-Up and Recording

For the calcium imaging, slices were infected with the calcium indicator AAV1.SYN.Gcamp6f.WPRE.SV40 [20] at one week after slicing. Twenty-four hours after infection the medium was changed. Calcium imaging was performed using a 20x magnification objective on an inverted microscope (Zeiss Axio Observer.Z1 Apotome.2) for living cell imaging, equipped with an AxioCam MRc camera, a chamber for CO_2 and temperature control for keeping same conditions as in cellular incubator. For imaging, the 24-well plate containing the slices from the same animal donor for the four different conditions (CNT, CNTWP, PTX, PTX-WP), were transferred to the microscope. The activity of each slice was then imaged for a duration of 20 minutes. One after the other all slices were imaged, and we did not follow any predefined sequence in the order of the slice to image in relation to the slice group. The plates were never opened, so the culturing conditions of the slices were always maintained to avoid any disturbance.

For the analysis of CNQX (6-cyano-7-nitroquinoxaline-2,3-dione)-D-AP5(DL-2-amino-5-phosphonopentanoic acid) the slices were first imaged for 10 minutes to get the basal activity, then CNQX/D-AP5 were added to the media, and after 30 minutes of incubation in controlled condition of temperature and CO2 (37°C and 5% CO2), the activity of each slice was again imaged for another 15 minutes.

Analysis of Calcium Imaging and Circuit Dynamics

Neuronal cell body segmentation was performed as described previously in [21]. Briefly, the maximum of each pixel across all calcium images acquired for a given slice was used to reconstruct the image template and to segment neuronal cells' contours through the custom-made software HIPPO. For each frame the average value of the pixels within a cell contour was calculated, and for each cell a calcium time series was then constructed across all frames. Time series were first high-pass filtered above 0.05 Hz to remove slow fluctuations and baseline changes, and next the traces were deconvolved using the MATLAB function "deconvolveCa" with default options, as derived and described from[22]. The onsets of the calcium events were extracted from the deconvolved calcium signal with start and end points set by the respective threshold of 0.05 and 0.04 ΔF/F (i.e. with a ratio of 1.25). The automatic detection of calcium spikes was later visually inspected for each cell. When the event detection was considered faulty, the starting and ending thresholds of a given calcium trace were adjusted manually always keeping respectively a ratio of 1.25 between them. A binary time series representing the calcium activity in each frame was first reconstructed for each cell where the ones marked the onset of calcium spikes. Given a cell, the interval between two consecutive onsets was used as instantaneous firing rate (IF). In order to calculate the firing correlation in each neuronal pair, the binary time series were smoothed with a Gaussian moving average using the MATLAB "smoothdata" function with a window length of 4 points and the correlation Cij was calculated as

$$C_{ij} = \frac{1}{\|x_i\| * \|x_j\|} * \sum_{t=1}^{T} x_i(t) * x_j(t) \qquad (1)$$

where $x_i(t)$ and $x_j(t)$ represent the time series of the neuronal pair (i,j), T the total number of frames (typically about 4800 for a 20 minute recording) and the symbol ‖ ‖ represents the norm of a vector (i.e. the time series $x_i(t)$ and $x_j(t)$).

Only for the case of assessing global synchronization, the binary time series $x_i(t)$ were smoothed with a different window length of 20, represented by $s_i(t)$, to address the dynamics emerging over larger time windows compared to the one from the neuronal pair. We calculated the global synchronization index at time t, $GSI(t)$, by summing over all network smoothed activity:

$$GSI(t) = \sum_{i=1}^{N} s_i(t) \qquad (2)$$

where N is the total number of imaged neurons. Network synchronizations (NSs) were identified by GSI exceeding a threshold of chance level with $p<0.05$, as calculated from a thousand reshuffled network dynamics where single neuron time series were randomized while keeping the same inter-event distribution in each neuron.

To each NS was assigned the timestamp of the peak of the corresponding GSI. All the cells recruited within a time window of seven frames around the GSI peak were considered as participating in the NS. The size of a NS event was calculated as the percentage of cells participating in a given NS out of the total number N of imaged neurons in the circuit.

The instantaneous frequency of NS in a given circuit was calculated as the inverse of the intervals (in seconds) between consecutive NSs.

The similarity between two NSs was calculated as the cosine between the two binary vectors A and B, ie.,

$$S_{AB} = \frac{1}{\|A\| * \|B\|} * \sum_{i=1}^{N} A_i * B_i \qquad (3)$$

where the vector components i are set to one if the neuron i is participating in the corresponding network synchronization, and zero otherwise.

Table 1 shows for each group and day of recording, and each slice, the imaged neurons per slice (ImN) and the number of network synchronizations (NS) occurred in the twenty minutes of recordings.

Immunostaining Protocol

At the end of the calcium imaging sessions, slices were washed with PBS and fixed with 4% paraformaldehyde for 30 min at room temperature. Immunohistochemical techniques were performed as described before [23,24]. Slices were incubated with blocking and permeabilization solution containing 0.25% Triton-X100 and 3% bovine serum albumin (BSA) in PBS for 3 h at room temperature, and then incubated overnight with the primary antibodies (diluted in the same solution) at 4ºC. After washing with PBS, the sections were incubated with fluorochrome-

conjugated secondary antibodies diluted in the permeabilization and blocking solution for 3h at room temperature. After washing with PBS, the sections were mounted on slides with Dako fluorescent mounting medium (Agilent-Dako S3023). The following primary antibodies were used: goat α-GFAP (Abcam Ab53554, 1:1,000); rabbit α-Iba 1 (Wako 19- 19741, 1:1000); mouse α-NeuN (MerkMillipore, MAB377, 1:1000); Rabbit α-GABA (GeneTex GTX125988, 1:1000); Rabbit α-GAD (Sigma-Aldrich G5163). The secondary antibodies used from ThermoFisher Scientific (1:1000), were: donkey α-rabbit Alexa Fluor 568 (A10043); donkey α -mouse Alexa Fluor 647 (A-31571); goat α -rabbit Alexa Fluor 488 (A-11034) and donkey α -goat Alexa Fluor 488 (A-21084). 4′,6-diamidino-2-phenylindole (DAPI, Sigma-Aldrich D9542).

Image Capture and Analysis of Immunostainings

All fluorescence images were collected employing a Leica Stellaris 5 (Leica, Wetzlar, Germany) microscope and LASAF software. Images were exported as tiffs and adjusted for brightness and background, using Adobe Photoshop ("levels" tool). All images shown are projections, from z-stacks of approximately 5 µm of thickness.

GABA/GAD Quantification

Quantitative analysis of cell populations was performed by design-based (assumption free, unbiased) stereology using a modified optical fractionator-sampling scheme[23,24]. All the quantifications regarding the GABAergic cell population are normalized to the number of NeuN+ cells (all neurons) in each slice. Therefore, we are quantifying the proportion of GABAergic cells within the total neuronal population.

Astrogliosis/Microgliosis

The area occupied by astrocytes was measured in the slices using the open-source FIJI (Image J). GFAP+ -cells were selected in z-stacks using the "Threshold" tool to outline the pixels of the image labeled with GFAP. "Measure" tool was used to calculate the % of occupied area by the staining in the image that have been highlighted before using the threshold [25]. Both measures were calculated from at least 5 z-stack from a minimum of three hippocampal slices.

Apoptosis

Apoptosis was quantified as previously described [25]. The number of pyknotic/ karyorrhectic

(condensed/fragmented DNA) nuclei were quantified in the granule cell layer + subgranular zone (GCL+SGZ).

Statistical Analysis

GraphPad Prism (Version 6 for Windows) was used for statistical analysis of figures 5 and 6. One-way ANOVA was performed in all cases to compare data from CNT, CNTWP, PTX and PTXWP in all the experiments. Error bars represent mean + standard error of the mean (SEM). Dots show individual data. To confirm the effect of the analysis, Student´s t test was carried out. Results are expressed as means ± SEM. Significant data are denoted with asterisks: *P < 0.05; **P < 0.01; ***P < 0.001.

MATLAB was used for the statistical analysis of the following variables quantifying networks' dynamics: single neuron firing rate, neuronal pair correlation, network synchronizations (size and frequency), and synchronizations' similarity.

The analysis was performed similarly in panel A of fig. 2, 3 and 5, and panel B and C of fig. 4, and supplementary fig. 1 and 2, using pooled datasets. Specifically, given a variable, all the data obtained from different slices belonging to a given experimental group (CNT, CNT-WP, PTX, PTX-WP) and day of experiment (3D, 7D, 10D) were pooled. Post-hoc statistical differences between groups were assessed using the Kruskall-Wallis's test for non-parametric group comparisons with corresponding p-values for each pair of groups. Corresponding plots represent for each group medians, 25-75% percentile limits, smallest-highest values, and outliers.

Panel B of fig 2, 3 and 5, and panel D and E of fig. 4 represent the cumulative distributions obtained as average across slices for a given experimental group and day of recording. Specifically, the range of the considered variable (from the smallest to the highest value) was equally divided into fifty intervals. For each slice the cumulative distribution of the variable was calculated on such intervals. The average cumulative distribution across slices was then calculated and plotted.

Panel C of fig. 2, 3 and 5 and panel F and G of fig. 4 plot the Kolmogorov-Smirnov statistics (KS-S) as a measure of distance between two experimental groups. Given a pair of experimental groups (out of CNT, CNT-WP, PTX and PTX-WP) the KS-S was calculated as the maximum difference between the corresponding cumulative distributions on each interval of the variable considered

(Smirnov 1939).

Data availability

The data that support the findings of this study are available from the corresponding author, upon reasonable request.

Results

Testing Epileptiform Activity by monitoring longitudinally Neuronal Firing in Organotypic Slices

In order to assess the impact of inhibiting STAT3 signalling pathway during epileptogenesis, we studied in-vitro hippocampal organotypic slices generated at P5-7 and cultured for at least 17 days (see Fig. 1A-B).

As a model of epileptogenesis, we exposed transitorily the circuits to hyper-excitation, by blocking GABAergic transmission through Picrotoxin (PTX), an antagonist of the GABA-A receptor. STAT3 pathway blockage was performed using WP1066, which inhibits the transcription of STAT3 gene [16]. We designed four experimental groups: a) control condition (CNT group), where cultured slices were never exposed to epileptogenesis or STAT-3 inhibition; b) epileptogenic condition (PTX group), where cultured slices underwent suppression of GABAergic transmission in extracellular presence of PTX (100 µM) from DIV12 to DIV14; c) epileptogenic and inhibited-STAT3 condition (PTX-WP group), where slices underwent suppression of GABAergic transmission as in the PTX group with simultaneous extracellular application of the STAT3 inhibitor WP-1066 (1,25 µM) and d) control under inhibited-STAT3 condition (CNT; CNT-WP group), where slices were exposed to WP1066 (1,25 µM) from DIV12 to DIV14. The slices obtained from the same animal (batch) were separated to cover the four different experimental conditions, cultured on the same multi-well plate, and imaged on the same DIV (see Methods). The effective need of a prolonged exposure (3 days) to GABAergic synaptic blockers to induce a sufficiently long epileptogenic time window leading to an impact on the dynamical states of the

slices was preliminarily verified (Supplementary Fig. 1A and B) in relation to single neuron and global circuits' dynamics, as described below in the corresponding sections of results.

To monitor longitudinally the activity of circuits, we expressed GCaMP6f only in neurons (with viral infection at 7 days in-vitro under the hSyn promoter, see Methods; Fig. 1B) and performed calcium imaging around the granular cell layer region (GCL; Fig. 1C) at 17, 21 and 24 days in-vitro (which correspond to 3, 7 and 10 days following the application of PTX/WP1066; Fig. 1B). The blockage of STAT3 expression using WP1066 was first checked by quantifying by RT-qPCR the mRNA levels of STAT3 at the third day of PTX exposure, under the different conditions (Fig. 1D). The treatment with PTX increases the expression of STAT3, while it was prevented by concomitant application of WP1066. Spontaneous circuit's dynamics were monitored simultaneously in several dozens of neurons over twenty minutes while fully preserving the culturing conditions. Following semi-automated cell contour segmentation and detection of calcium spikes, the onsets of calcium events were extracted from each neuronal trace in order to reconstruct circuits' dynamics from single neuron firing properties to pair and ensemble synchronizations (Fig. 1E-G). In addition, at 3D, 7D and 10D slices were stained for the immunochemical characterization of the glial neuroinflammatory state of cellular alterations (i.e. counting alive/apoptotic cells and GABAergic cell density in the GCL; Fig. 1F, 6 and 7). The density of live cells was used to monitor the health of the organotypic cultures (Fig 1F). As expected, there is a progressive decrease of cell density with time in culture[26].

Blockage of STAT-3 Restores Neuronal Firing in Epileptogenic conditions

We first focused on single neuron dynamics and in each neuron, we calculated the instantaneous frequency of calcium events (*IF*, i.e. the inverse of the time interval between consecutive calcium spikes) as an indicator of neural firing frequency and general circuits' excitability. The effective need of a prolonged exposure (3 days) to GABAergic synaptic blockers to impact neural firing was preliminarily verified. The application of PTX just for 1 day slightly increased at 3D the average neural firing frequency compare to control condition (0.06 and 0.04 Hz in PTX and in control respectively; Supplementary Fig. 1A). However, 3 days of PTX exposure significantly

increased 3 times the average neural firing frequency compared to 1day of PTX exposure 0.18 Hz for 3 days PTX exposure; Supplementary Fig. 1B). To further confirmed our model we imaged the slices in presence of PTX (in 3rd day of exposure) and also at 3D (i.e. 3 days after the PTX wash-out). The hyper-excitable epileptic-like state in presence of PTX was characterized by an average neural firing frequency of 0.15 Hz, significantly higher than the corresponding control condition. Therefore, the average neural firing frequency was significantly increased compared to corresponding baseline conditions both in presence of PTX and similarly 3 days after the wash-out of PTX (Supplementary Fig. 1C). Baseline control activity and hyper-active neural firing observed in PTX treated slices at 3D was abolished in presence of glutamatergic synaptic blockers (CNQX 20μM and D-AP5 10μM blocking AMPA/Kainate and NMDA receptors respectively), confirming that baseline activity and higher neural firing induced by long PTX exposure are grounded on glutamatergic transmission (Supplementary Fig. 1D). Given the above observations, we used 3 days of PTX treatment in order to have a clear impact after the wash out of the GABAergic blocker

We next focused on single neuron dynamics under the four different experimental conditions at 3D, 7D and 10D (Fig. 2) after PTX exposure. We imaged an average of 98+/-22 neurons across all experimental conditions as summarized in the table 1, on a total of N=60 slices. The comparison of single neuron firing frequency between groups (and similarly to other neural dynamics variables shown in figure 3, 4 and 5) was done both on the values of IF pooled across all slices and neurons (obtaining one global distribution per group; panel 2A) and on the average cumulative distributions of IF across slices (panel 2B and C), as described below.

After pooling *IFs* across all neurons from all slices within the same group and day of recording (N>=325, see table 1), non-parametric group comparison (Kruskal-Wallis test, see Methods) revealed a significant difference at 3D, 7D and 10D between the PTX-group and all other groups (Fig. 2A). Although differences in some cases could be detected also between other groups, the median IF of the PTX-group (Fig. 2A, red horizontal line in the bar plots) was always the highest.

Further quantification of the statistical difference between the groups was performed using the distance between average cumulative distributions (in this case data were not pooled but averaged across slices, and therefore a representative average cumulative distribution for each group and recording day was reconstructed; see Methods and Fig. 2B). We used as a metric of distance (i.e.

difference) between groups the Kolmogorov-Smirnov statistics (KS-S), i.e. the maximum difference between cumulative distributions (Fig. 2C). The KS-S values between the epileptic group (PTX) and all other groups (CNT, PTX-WP and CNT-WP; see red dots in Fig. 2C) were always (i.e. at 3D, 7D and 10D) higher when compared to the distance between the other groups (blue dots).

Summarizing the results, the higher levels of single-neuron firing in the circuits exposed to epileptogenic conditions (PTX group) confirm the induction of a hyper-excitable epileptic-like state. Importantly, the acute inhibition of the STAT3 restores the level of single-neuron firing to baseline control conditions.

Blockage of STAT3 preserve physiological Neuronal Pair-Wise dynamics

Since ictal and inter-ictal epileptic dynamics are characterized by pathological synchronous events across neurons and brain circuits, next, we looked at the coordinated firing across cells in the circuits, focusing first on the neuronal pairs' level. Physiologically, communication between neuronal pairs leads to correlated neuronal pair activity. However, synchronous epileptic dynamics could emerge from pair-wise level scaling up to circuits. Therefore, we expected higher pair-wise correlation in the spontaneous firing of epileptic circuits.

Therefore, we calculated the correlation between the smoothed time series of neuronal firing (see Fig. 3 and Methods).

Non-parametric group comparison on pooled statistic of firing's correlations across all neuronal pairs and slices showed significant differences between all groups at 3D, 7D and 10D (Fig 3A). Note that the statistic on neuronal pairs scales as the square of number of neurons, therefore the number of pooled observations in each group and recording day was very high (>17530 neuronal pairs) compared to single neuron statistics. At 3D the median of firing's correlations in the PTX-group was remarkably higher (>33%) when compared to the other cases (0.52 in PTX, 0.39 in CNT, 0.23 CNT-WP and 0.34 in PTX-WP group respectively). Also, at 3D the KS-S revealed

higher differences between the epileptic group compared to other groups as shown in Fig 3B and C. The same trend but attenuated was observed at 7D with higher pair correlation (>11%; 0.30 PTX, 0.22 CNT, 0.18 CNT-WP, 0,27 PTX-WP group) and higher KS-S when comparing the PTX-group compared to the others. At 10D both medians of IF and KS-S differences showed similar values when comparing groups. Summarizing the results, higher levels of pair-wise synchronized dynamics were observed in the epileptic group at 3D and 7D, but not at 10D (when also the density of alive cells in the circuits displayed lowest values, as previously shown in see Fig. 1E).

Blockage of STAT3 Restores Neuronal Ensemble Synchronization

Since synchronization is a key feature of epileptic activity, but also a physiological feature of spontaneous circuit dynamics, next, we quantified networks' synchronizations (NS, Fig. 4). Since synchronized events could also be detected by chance simply as a consequence of the background neuronal activity, we considered here only synchronizations with a number of recruited cells above chance level (Fig. 4A), the latter estimated from reshuffled random firing keeping same firing frequency in single neuron (see Methods). Similarly to the single neuron firing, we first verified that a prolonged exposure (3 days) to GABAergic synaptic blockers endured a sufficiently long epileptogenic time window leading to an impact on networks' synchronizations (Supp. Fig 2). When looking at the frequency of circuits' synchronization for slices treated only 1 day with PTX, we did not observe any significant increase in the frequency of circuit synchronizations compared to corresponding control conditions (supplementary fig. 2A). On the contrary a significant increase in the synchronization frequency was observed when slices were treated for 3 days with PTX (supp. Fig. 2B). Notably a similar increase in the frequency of synchronizations was observed in presence of PTX (i.e. the disinhibited epileptic condition; supp. Fig. 2C).

Next, we quantified the instantaneous frequency (panels 4B, D and F) and the size (panels 4C, E and G) of the synchronizations, the latter quantified as percentage of recruited cells within the imaged neural population.

The pooled statistics of circuits' synchronizations showed similar trends at 3D and 7D. Specifically non-parametric statistics showed that PTX-groups were significantly different to all other groups in terms of frequency and size of circuits synchronization ($p<0.05$) while all other groups did not show significant differences between them). Higher frequency of synchronizations (medians at 3D and 7D of PTX-group were 0.11 and 0.09 Hz respectively, while all other groups had median

values of 0.07 Hz) and percentage of recruited neurons in synchronized events (medians of groups at 3D: PTX 76.8%, CNT 46.6%, CNT-WP 46.8%, PTX-WP 52.7%; medians of groups at 7D: PTX 57%, CNT 42.0%, CNT-WP 40.8%, PTX-WP 42.9%) were observed in the PTX-group compared to the other groups. Similarly, at 3D and 7D, the KS-S showed higher differences between the PTX-group and all other groups (Fig. 4B and C). At 10D, such trends were not observed anymore, and the pooled statistics revealed a significant difference between CNT and all other groups in terms of synchronizations frequency (Fig. 4C), while in terms of synchronization size all groups were significantly different apart the case of CNT vs. PTX and CNT-WP vs. PTX-WP (Fig. 4 D). At 10D also the KS-S did not show the previously trends observed at 3D and 7D. Summarizing the results, synchronized ensemble dynamics in the epileptic group were more frequent and recruited a larger number of neurons at 3D and 7D, while at 10D such trends did not persist.

Given that epileptic circuits present dysfunctional topological organizations with hypersynchronous patterns, to characterize the complexity of spontaneous ensemble dynamics in terms of the richness of repertoire of synchronization patterns generated by the circuits, we observed the similarity between the circuit synchronizations (Fig. 5). The underlying hypothesis is that in a dysfunctional circuit a reduced complexity should be observed in the generated patterns and dynamics. We quantified the similarity of the generated synchronized patterns as the cosine of the angle between the binary vectors representing the neurons recruited in the circuits' synchronizations (see Methods). The pooled statistics revealed significant differences between all groups at 3D, 7D and 10D (Fig. 5A). Note that also in this case, as in neuronal pairs correlation, the number of observations (>3008 pairs of synchronization) scales as the square of the total number of synchronizations. At 3D the median similarity of the synchronizations generated in the PTX group was very high (median 0.89 out of a possible maximum of 1) compared to the other groups (0.57 CNT, 0.57 CNT-WP and 0.64 PTX-WP). The gap was attenuated at 7D (0.63 PTX, 0.49 CNT, 0.57 CNT-WP and 0.52 PTX-WP). KS-S showed clearly how the distribution of events both at 3D and 7D in the PTX group was consistently more distant to all other groups (Fig 5 B and C). All the above trends on the similarity of synchronizations patterns were not present at 10D.

Blockage of STAT3 prevents gliosis and loss of GABAergic cells in epileptogenic conditions

The PTX-group showed stereotypical patterns of hyperexcitable epileptic states from single neuron firing to increased pair-wise correlations and larger ensembles' synchronizations. These alterations were attenuated in general by the inhibition of STAT-3. We therefore tested whether this beneficial effect could be mediated by a reduction in neuroinflammation and preservation of interneurons (i.e. GABAergic neurons). We first, performed immunostaining to quantify the density of apoptotic cells and of inhibitory neurons (i.e. GABAergic cells). Coherently with the reported literature [27–29] on the loss of GABAergic neurons across the development and installment of epilepsy, we hypothesized that: 1) PTX induce the loss of GABA cells leading to hyper-excitable circuits' states, and that 2) inhibition of STAT3 during the time window of epileptogenesis reduced cellular damage impacting on the emergence of epileptic circuit dynamics (Fig. 2-4).

Therefore, we quantified the number of GABA-positive cells in the GCL, out of whole population of neurons (NeuN-positive cells; Fig. 6A). At 3D we saw that the presence of GABA cells in the epileptic group was reduced to a 2%, about 50% less when compared to all other conditions, in which the GABAergic population represented about 4% of the overall neural population (Fig. 6B). Similar results additionally characterized were obtained at 7D (central plot of Fig. 6B), although with a general decrease in all conditions in the GABAergic population (more pronounced in the PTX-WP group with values around 3%). Also, at 10D we observed under all conditions a general decrease of the percentage of GABAergic neurons, but still maintaining the trend of 3D and 7D with lowest values observed in the PTX-group (right plots of Fig. 6 B). We further confirm these results by using GAD antibody (Supplementary Fig. 3A). The quantification of GAD-positive cells in the GCL across the different experimental conditions at 3D presented the same trend displayed when using the GABA antibody, although with slight lower values of density (Supplementary Fig. 3B).

Since GABAergic cells presence was reduced under epileptic conditions but preserved by the acute blockage of the STAT3, next we looked at overall cell loss, and we quantified the presence of dead cells at 3, 7 and 10D counting the number of apoptotic cells GCL+SGZ (see Methods) as a readout of cellular damage through the nuclear staining DAPI (Fig. 6C). We found that at 3D and 7D cell loss was higher in the epileptic group, with a higher significant ratio of apoptotic cells compared

to the other conditions. This result highlights a general circuit structural damage in the epileptic group. The inhibition of STAT3 under epileptogenesis (PTX-WP group) prevented general cellular damage. At 10D whole experimental group showed similar presence of dead cells, but this also corresponded to lowest and similar densities of live cells in the cultures (as previously shown in Fig. 1E).

Overall, the above immuno-characterizations showed that epileptic conditions induce a general loss of cells targeting preferentially the GABAergic neuronal population which is decreased to half of the baseline levels, and that anti-inflammatory conditions prevent both overall cell loss and specifically of GABAergic cells.

Since we studied the impact on the epileptogenic conditions of inhibiting the STAT3-mediated response, next we characterized the inflammatory profile of the circuit in the different glial populations. Reactive glia, involving both astrocytes and microglia, is one of the hallmarks of the epilepsy. We first focused on reactive astrogliosis measuring the overall area occupied by GFAP staining at 3D, 7D and 10D, as overexpression of GFAP represents a hallmark of reactive astrocytes (Fig. 7A). At 3D, 7D and 10D the expression of GFAP was significantly higher in the PTX group compared to all other groups, (Fig. 7B). However, the inhibition of STAT3 significantly reduced the area occupied by GFAP to control levels.

Next, we tested the reactivity of the microglia cells, using the specific microglial marker Iba1 (Fig. 7C). Similarly, to what we observed for astrocytes, we found that the expression of Iba1, as measured by the area occupied by the marker, was significantly increased in the PTX group compared to all other groups at 3D, 7D and 10D (Fig. 7D). The blockage of STAT-3 reduced the area occupied by Iba1 to control levels.

Our previous results on glial reactivity show that STAT3 transcription inhibition alone was able to prevent the reactivity response of both astrocytes and microglial cells under epileptogenic conditions.

The overall immunostaining characterizations of the structural and inflammatory profiles of the circuits show that hyperexcitable conditions induce a general reactive gliosis accompanied by an increase in the number of apoptotic cells with a greater loss in GABAergic population, which are

stereotypical hallmarks of epileptic states. Notably, we emphasize again that the sole inhibition of STA3 transcription was capable to prevent the induction of these epileptic markers.

Discussion

We used organotypic hippocampal cultures as an in-vitro model of temporal lobe epilepsy, similarly to what previously described in literature [17,18,30.] We exposed transitorily cultured circuits to pro-epileptic hyper-excitable conditions by suppressing GABAergic synaptic transmission to model epileptogenesis. Preliminarily, we report that a prolonged exposure to GABAergic synaptic blocker PTX (3 days of treatment) was effective and needed to observe a clear impact on neural dynamics. This effect is not achieved when the slices were exposure to PTX for just 1 day. Using calcium imaging to monitor spontaneous neural dynamics simultaneously on dozens of neurons from 3 to 10 days following epileptogenic episodes, we observed that at 3D and 7D monitored circuits displayed increased single neuron firing, increased firing correlations in neural pairs, higher frequency of circuits' synchronizations with higher number of recruited neurons and decreased complexity of synchronized patterns (i.e. a less rich repertoire of activity as reflected by higher similarity between generated patterns). In addition, in agreement with previous results on epileptic circuits, we also observed increased cellular loss [26]and in particular with respect to the GABAergic population [28].

It is known that the pattern of expression of organization of GABAergic cells in developmental circuits resembling adult conditions is observed not before P10[31,32]. This is a key point to understand the percentage of GABAergic cell obtained in our experimental model as it is based on slices extracted at P5-7

Therefore, a lower presence of inhibitory cells was present in the epileptic circuits, favouring the appearance of hyperexcitable states with increased frequency of single cell and coordinate circuit's activity. Moreover, epileptic circuits showed a persistent inflammatory glial profile as revealed by astrocytic and microglial markers

Although such observations on in-vitro hippocampal slices are in general agreement with previous literature [30,33], to the best of our knowledge this is the first time that spontaneous synchronizations and emergent collective dynamics were consistently studied and quantified in epileptic circuits

longitudinally along days after epileptogenesis. This was very possible by maintaining the culturing conditions during the imaging sessions in undisturbed conditions, avoiding the perfusion of extracellular ACSF or medium which is a major protocol used in previous works [18].

When we selectively blocked STAT3[34], concomitantly during the time windows of epileptogenesis (by simultaneous application of PTX and WP1066), we observed that epileptic dynamics, cellular loss, GABAergic cells depletion, and reactive gliosis were not present in the neuro-glial circuits, with variable values at baseline control levels. This was clear longitudinally at 3 and 7 days following the episode of epileptogenesis while at 10 days no clear differences and trends could be observed anymore.

The general loss of difference between the experimental conditions at 10D both in terms of circuits dynamics, GABAergic density and neuro-inflammatory profile, can be explained by the progressive cell loss and decreased density of alive cells in the cultured circuits, which was occurring in both control conditions and in all other tested conditions. Although at 10D the level of apoptosis in all groups is similar, importantly the composition on the neuronal population can play a role, since the GABAergic population has been preserved with the treatment (WP1066).

It was described that the time in culture directly impacts the integrity and viability of the cultured slices[26] with the period from DIV7 to DIV14, being of particular vulnerability, and eventually the slices cannot be maintained alive past a few weeks. Organotypic hippocampal slices are commonly used as an in vitro model of seizures and chronic epilepsy [17]. Here we demonstrate that PTX-treated organotypic cultures recapitulate the most typical features of epileptogenesis: spontaneous electrical seizures, cell death, inflammation, and alteration of neuronal circuitry, as previously described by other authors [30,33]. Although there is some controversy about the intrinsic epileptic profile of organotypic slices even under control conditions [35], our results demonstrated that PTX-treated organotypic slices are an excellent model to study and understand epileptogenesis. Indeed, when we imaged slices under commonly used conditions, i.e. by perfusion of ACSF losing culture conditions, we did not observe spontaneous synchronizations (unshown).

Here we focused on the role of STAT3 in the development of epilepsy and neuroinflammation. The JAK/STAT3 pathway is known to be rapidly activated in the hippocampus after status epilepticus[36]. Previous reports linked STAT3 activation to epileptogenesis [37], suggesting that STAT3 remains activated up to 1 month, maintaining and aggravating the effect of astrogliosis [15].

STAT3 could thus promote spontaneous seizures by contributing to reactive gliosis triggered by the initial event. STAT3 can be pharmacologically blocked by different drugs such as Pyridone or WP1066. It was shown that STAT3 blocked by WP1066 lowered the number of spontaneous seizures in a rat pilocarpine model of epilepsy reducing the severity of subsequent seizures [16].

We herein extend some of these results, and show that inhibition of STAT3 with WP1066 not only reduced the effect of epilepsy on the neuronal circuits' functionality, but this strategy also precisely preserved the topology of the circuit. We show that the alteration of the neuronal circuits is accompanied by topological changes such as the loss of GABAergic cells. We observed that the number of GABAergic cells decreased in comparison to control condition in all time points. Interestingly, this loss of GABAergic cells has been shown in-vivo TLE induced models by pilocarpine [28]. The role of GABAergic neurons in the development and prevalence of epilepsy has been extensively studied in animal models, demonstrating that GABAergic interneuron loss can change the excitation/inhibition balance. In this work, we have shown for the very first time that STAT3 blockage reduces GABAergic cell loss in an in-vitro model of epilepsy.

Neuroinflammation is another hallmark of epilepsy; therefore, we resorted to analyse the inflammatory profile of the organotypic slices. Gliosis includes both reactive astrocytes and reactive microglia, as astrocytes and microglia are interconnected such that the activity of one cell type affects the activity of the other [27,38–40]. Here, gliosis was measured by the area occupied by astrocytes and microglia. Our results confirm the previous results in which STAT3 inhibition reduced GFAP and Iba1 overexpression after epilepsy [15]. Thus, we have shown that STAT3 inhibition could impact the activation of astrocytes and microglia in the epileptogenic process.

Our data suggest that the JAK/STAT inhibition at the onset of the epileptic event could modify the progress of epilepsy. Inhibition of this pathway may open up novel therapeutic possibilities as a complement to other commonly used anticonvulsant drugs.

Acknowledgements

We thank prof. Juan Manuel Encinas for his comments and insights.

Funding

This work was supported by with FEDER Funds (AI-2021-039), Spanish Ministry of Science and Innovation ("ministerio de ciencia y innovación ;PID2021-127163NB-I00) and the Ikerbasque start-up funding. SM-S received a Juan de la Cierva-formación Fellowship (FJC2018-035496-I) and later a HPC&Ai-IKUR (Basque Government) Postdoctoral Fellowship.

Competing interests

The authors report no competing interests.

Supplementary material

Supplementary material is available at *Brain* online.

References

1. Covolan L, Mello LEAM. Temporal profile of neuronal injury following pilocarpine or kainic acid-induced status epilepticus. *Epilepsy Res*. 2000;39(2):133-152. doi:10.1016/S0920-1211(99)00119-9
2. Curia G, Longo D, Biagini G, Jones RSG, Avoli M. The pilocarpine model of temporal lobe epilepsy. *J Neurosci Methods*. 2008;172(2):143-157. doi:10.1016/j.jneumeth.2008.04.019
3. Fujikawa DG. The temporal evolution of neuronal damage from pilocarpine-induced status epilepticus. *Brain Res*. 1996;725(1):11-22. doi:10.1016/0006-8993(96)00203-X
4. Lévesque M, Avoli M, Bernard C. Animal models of temporal lobe epilepsy following systemic chemoconvulsant administration. *J Neurosci Methods*. 2016;260:45-52. doi:10.1016/j.jneumeth.2015.03.009
5. Stephen LJ, Kwan P, Brodie MJ. Does the Cause of Localisation-Related Epilepsy Influence the Response to Antiepileptic Drug Treatment? *Epilepsia*. 2001;42(3):357-362. doi:10.1046/j.1528-1157.2001.29000.x
6. Duncan. doi:10.1016/S0140-6736(06)68477-8 | Elsevier Enhanced Reader. doi:10.1016/S0140-

6736(06)68477-8

7. Brodie MJ, Barry SJE, Bamagous GA, Norrie JD, Kwan P. Patterns of treatment response in newly diagnosed epilepsy. *Neurology*. 2012;78(20):1548-1554. doi:10.1212/WNL.0b013e3182563b19

8. Macdonald RL, Kelly KM. Antiepileptic Drug Mechanisms of Action. *Epilepsia*. 1995;36(s2):S2-S12. doi:10.1111/j.1528-1157.1995.tb05996.x

9. Rogawski MA, Löscher W, Rho JM. Mechanisms of Action of Antiseizure Drugs and the Ketogenic Diet. *Cold Spring Harb Perspect Med*. 2016;6(5):a022780. doi:10.1101/cshperspect.a022780

10. Vezzani A, French J, Bartfai T, Baram TZ. The role of inflammation in epilepsy. *Nat Rev Neurol*. 2011;7(1):31-40. doi:10.1038/nrneurol.2010.178

11. Quirico-Santos T, Meira ID, Gomes AC, et al. Resection of the epileptogenic lesion abolishes seizures and reduces inflammatory cytokines of patients with temporal lobe epilepsy. *J Neuroimmunol*. 2013;254(1-2):125-130. doi:10.1016/j.jneuroim.2012.08.004

12. Ghoreschi K, Jesson MI, Li X, et al. Modulation of Innate and Adaptive Immune Responses by Tofacitinib (CP-690,550). *J Immunol Baltim Md 1950*. 2011;186(7):4234-4243. doi:10.4049/jimmunol.1003668

13. Nicolas CS, Peineau S, Amici M, et al. The Jak/STAT pathway is involved in synaptic plasticity. *Neuron*. 2012;73(2):374-390. doi:10.1016/j.neuron.2011.11.024

14. Nicolas CS, Amici M, Bortolotto ZA, et al. The role of JAK-STAT signaling within the CNS. *JAK-STAT*. 2013;2(1):e22925. doi:10.4161/jkst.22925

15. Xu Z, Xue T, Zhang Z, et al. Role of Signal Transducer and Activator of Transcription-3 in Up-Regulation of GFAP After Epilepsy. *Neurochem Res*. 2011;36(12):2208-2215. doi:10.1007/s11064-011-0576-1

16. Grabenstatter HL, Angel YCD, Carlsen J, et al. The effect of STAT3 Inhibition on status epilepticus and subsequent spontaneous seizures in the Pilocarpine Model of Acquired Epilepsy. *Neurobiol Dis*. 2014;62:73-85. doi:10.1016/j.nbd.2013.09.003

17. Abiega O, Beccari S, Diaz-Aparicio I, et al. Neuronal Hyperactivity Disturbs ATP Microgradients, Impairs Microglial Motility, and Reduces Phagocytic Receptor Expression Triggering Apoptosis/Microglial Phagocytosis Uncoupling. *PLOS Biol*. 2016;14(5):e1002466. doi:10.1371/journal.pbio.1002466

18. Stoppini L, Buchs PA, Muller D. A simple method for organotypic cultures of nervous tissue. *J Neurosci Methods*. 1991;37(2):173-182. doi:10.1016/0165-0270(91)90128-M

19. Cronberg T, Rytter A, Asztély F, Söder A, Wieloch T. Glucose but Not Lactate in Combination With Acidosis Aggravates Ischemic Neuronal Death In Vitro. *Stroke*. 2004;35(3):753-757. doi:10.1161/01.STR.0000117576.09512.32

20. Dana H, Sun Y, Mohar B, et al. High-performance calcium sensors for imaging activity in neuronal populations and microcompartments. *Nat Methods*. 2019;16(7):649-657. doi:10.1038/s41592-019-0435-6

21. Kanner S, Goldin M, Galron R, Ben Jacob E, Bonifazi P, Barzilai A. Astrocytes restore connectivity and synchronization in dysfunctional cerebellar networks. *Proc Natl Acad Sci*. 2018;115(31):8025-8030. doi:10.1073/pnas.1718582115

22. Friedrich J, Zhou P, Paninski L. Fast online deconvolution of calcium imaging data. *PLOS Comput Biol*. 2017;13(3):e1005423. doi:10.1371/journal.pcbi.1005423

23. Encinas JM, Enikolopov G. Identifying and quantitating neural stem and progenitor cells in the adult brain. *Methods Cell Biol*. 2008;85:243-272. doi:10.1016/S0091-679X(08)85011-X

24. Encinas JM, Michurina TV, Peunova N, et al. Division-coupled astrocytic differentiation and age-related depletion of neural stem cells in the adult hippocampus. *Cell Stem Cell*. 2011;8(5):566-579. doi:10.1016/j.stem.2011.03.010

25. Martín-Suárez S, Abiega O, Ricobaraza A, Hernandez-Alcoceba R, Encinas JM. Alterations of the Hippocampal Neurogenic Niche in a Mouse Model of Dravet Syndrome. *Front Cell Dev Biol*. 2020;8:654. doi:10.3389/fcell.2020.00654

26. Li F, Song Y, Dryer A, Cogguillo W, Berdichevsky Y, Zhou C. Nondestructive evaluation of progressive neuronal changes in organotypic rat hippocampal slice cultures using ultrahigh-resolution optical coherence microscopy. *Neurophotonics*. 2014;1(2):025002. doi:10.1117/1.NPh.1.2.025002

27. Ben-Ari Y, Represa A. Brief seizure episodes induce long-term potentiation and mossy fibre sprouting in the hippocampus. *Trends Neurosci*. 1990;13(8):312-318. doi:10.1016/0166-2236(90)90135-W

28. Knopp A, Frahm C, Fidzinski P, Witte OW, Behr J. Loss of GABAergic neurons in the subiculum and its functional implications in temporal lobe epilepsy. *Brain*. 2008;131(6):1516-1527.

doi:10.1093/brain/awn095

29. Houser CR. Do Structural Changes in GABA Neurons Give Rise to the Epileptic State? *Adv Exp Med Biol*. 2014;813:151-160. doi:10.1007/978-94-017-8914-1_12

30. Stoppini L, Duport S, Corrèges P. A new extracellular multirecording system for electrophysiological studies: application to hippocampal organotypic cultures. *J Neurosci Methods*. 1997;72(1):23-33. doi:10.1016/S0165-0270(96)00151-3

31. Ben-Ari Y, Rovira C, Gaiarsa JL, Corradetti R, Robain O, Cherubini E. Chapter 23 Chapter GABAergic mechanisms in the CA3 hippocampal region during early postnatal life. In: *Progress in Brain Research*. Vol 83. Elsevier; 1990:313-321. doi:10.1016/S0079-6123(08)61259-5

32. Rozenberg F, Robain O, Jardin L, Ben-Ari Y. Distribution of GABAergic neurons in late fetal and early postnatal rat hippocampus. *Dev Brain Res*. 1989;50(2):177-187. doi:10.1016/0165-3806(89)90193-4

33. Duport S, Stoppini L, Corrèges P. Electrophysiological approach of the antiepileptic effect of dexamethasome on hippocampal slice culture usihg a multirecording system: The physiocard®. *Life Sci*. 1997;60(17):PL251-PL256. doi:10.1016/S0024-3205(97)00104-5

34. Iwamaru A, Szymanski S, Iwado E, et al. A novel inhibitor of the STAT3 pathway induces apoptosis in malignant glioma cells both in vitro and in vivo. *Oncogene*. 2007;26(17):2435-2444. doi:10.1038/sj.onc.1210031

35. Liu J, Saponjian Y, Mahoney MM, Staley KJ, Berdichevsky Y. Epileptogenesis in organotypic hippocampal cultures has limited dependence on culture medium composition. *PLOS ONE*. 2017;12(2):e0172677. doi:10.1371/journal.pone.0172677

36. Raible DJ, Frey LC, Brooks-Kayal AR. Effects of JAK2-STAT3 signaling after cerebral insults. *JAK-STAT*. 2014;3(2):e29510. doi:10.4161/jkst.29510

37. Okamoto OK, Janjoppi L, Bonone FM, et al. Whole transcriptome analysis of the hippocampus: toward a molecular portrait of epileptogenesis. *BMC Genomics*. 2010;11(1):230. doi:10.1186/1471-2164-11-230

38. Sanz P, Garcia-Gimeno MA. Reactive Glia Inflammatory Signaling Pathways and Epilepsy. *Int J Mol Sci*. 2020;21(11):4096. doi:10.3390/ijms21114096

39. Cohen I, Navarro V, Clemenceau S, Baulac M, Miles R. On the Origin of Interictal Activity in Human Temporal Lobe Epilepsy in Vitro. *Science*. 2002;298(5597):1418-1421. doi:10.1126/science.1076510

40. Knopp A, Kivi A, Wozny C, Heinemann U, Behr J. Cellular and network properties of the subiculum in the pilocarpine model of temporal lobe epilepsy. *J Comp Neurol*. 2005;483(4):476-488. doi:10.1002/cne.20460

Figure legends

Figure 1 Experimental model, longitudinal calcium imaging and immunostaining. (**A**) Scheme of the positive feedback loop mechanism where seizures lead to more seizures through complex interactions which involve gliosis and neuroinflammation ultimately leading to pathotopological organization of neuroglial circuit. (**B**) Scheme of the experimental procedure. The organotypic slices (OTC) were extracted at P-5-7 (d0) and cultured. After 7 days (d7) slices are infected for the expression of the GCaMP6f. From d12 to d14 slices are exposed to PTX and/or WP1066. Imaging and immunostaining are performed 3-7-10 days after (i.e. at d17-21-24, we refer to them respectively as 3D, 7D and 10D). (**C**) Representative image acquired at 10x of the cells expressing the calcium sensor at d17. Note that imaging of the neurons was performed in a forth of the field shown, in correspondence of the granular cell layer region. (**D**) Quantification of STAT3 levels by RT-qPCR at the 3rd day of PTX exposure. (**E**) Representative calcium traces of 7 neurons from a control slice at d17 with zoomed visualization (gray shaded) of the calcium traces and spikes' onsets highlighted by black markers. (**F**) Health state of the circuits assessed by the density of alive cells per mm^3. (**G**) Representative raster plots (top row) showing the calcium spikes' onsets of each cell over time in the four experimental group at d17. The percentage of active cell per frame is plotted in the bottom panels.

Figure 2 Single neuron level: frequency of calcium events. For each cell the average inverse of the intervals between consecutive calcium spikes are considered as firing rate. From left to right, results from slices respectively at 3, 7 and 10D are shown. (**A**) Pooled values at 3-7-10D across all slices are showing median (horizontal line) 25-75 percentile limits, bottom-top range values and outliers (marked by red asterisks). (**B**) Cumulative distributions obtained as average across slices belonging to same condition. Fifty identical equally sized intervals were chosen within the minimum-maximum range of the variable across all groups. (**C**) Maximum difference between

cumulative distributions shown in B (KS-S) for all group comparisons. Red dots highlight the comparison in the PTX-group vs. all other groups. All other comparisons are shown as blue dots. Significant data are denoted with asterisks: *P < 0.05; **P < 0.01; ***P <0.001.

Figure 3 Pair-wise level: firing correlation in neuronal pairs. (**A**) Pooled values at 3-7-10D across all slices of the firing correlation are showing median (horizontal line) 25-75 percentile limits, bottom-top range values and outliers (marked by red asterisks). (**B**) Cumulative distributions obtained as average across slices belonging to same conditions. Fifty identical equally sized intervals were chosen within the minimum-maximum range across all groups. (**C**) Maximum difference between cumulative distributions shown in B (KS-S) for all group comparisons. Red dots highlight the comparison in the PTX-group vs. all other groups. All other comparisons are shown as blue dots. Significant data are denoted with asterisks: *P < 0.05; **P < 0.01; ***P < 0.001.

Figure 4 Ensemble level: size and frequency of circuits' synchronizations. For panels B-G, a similar plot scheme to Fig.2 and 3 was used. (**A**) Representative zoomed raster plot (top) of the smoothed calcium spikes' onsets and the sum per frame of the activity (bottom). The asterisks mark synchronizations whose sizes are above chance level (marked as a horizontal line) (**B, C**) Pooled values of synchronizations' sizes (**B**) and frequencies (**C**) at 3-7-10D across all slices are showing median (horizontal line) 25-75 percentile limits, bottom-top range values and outliers (marked by red asterisks). (**D, E**) Cumulative distributions of synchronizations' sizes (**D**) and frequencies (**E**) obtained as average across slices belonging to same conditions. Fifty identical equally sized intervals were chosen within the minimum-maximum range across all groups. (**F, G**) Maximum differences (KS-S) between cumulative distributions shown in (**D**) (panel F) and (**E**) (panel **G**) for all group comparisons. Red dots highlight the comparison in the PTX-group vs. all other groups. All other comparisons are shown as blue dots. Significant data are denoted with asterisks: *P < 0.05; **P < 0.01; ***P < 0.001.

Figure 5 Ensemble level: similarity between circuits' synchronizations. Similar plot scheme

to Fig.2 and 3. (**A**) Pooled values at 3-7-10D across all slices are showing median (horizontal line) 25-75 percentile limits, bottom-top range values and outliers (marked by red asterisks). (**B**) Cumulative distributions obtained as average across slices belonging to same conditions. Fifty identical equally sized intervals were chosen within the minimum-maximum range across all groups. (**C**) Maximum difference between cumulative distributions shown in B (KS-S) for all group comparisons. Red dots highlight the comparison in the PTX-group vs. all other groups. All other comparisons are shown as blue dots.

Figure 6 Characterization of circuits' composition through GABAergic and apoptotic cell density: WP1066 prevents cell loss and death of GABAergic neurons. (**A**) Representative confocal microscopy images showing GABA positive cells in the granule cell layer in the different conditions at 3, 7 and 10 days. (**B**) Quantification of the proportion of GABA/NeuN positive cells among the total number of NeuN positive cells at 3, 7 and 10 days after the addition of PTX/WP1066. (**C**) Quantification of the proportion of apoptotic cells in the slices at 3, 7 and 10 days after the addition of PTX/WP1066. Scale bar is 10 μm. One-way ANOVA after all pair-wise multiple comparisons by Holm-Sidak post hoc test. Bars show mean ± SEM. Dots show individual data. *$p < 0.05$, **$p < 0.01$, ***$p < 0.001$.

Figure 7 Circuits' neuro-inflammatory profile: WP1066 prevent the glial inflammatory state which is present in epileptic circuits. (**A**) Representative confocal microscopy images showing the area occupied by the astrocytic marker GFAP in the different conditions at 3, 7 and 10 days. (**B**) Quantification of area occupied by GFAP at 3 days, 7 days and 10 days after the addition of PTX/WP1066. (**C**) Quantification of area occupied by Iba1 at 3 days, 7 days and 10 days after the addition of PTX/WP1066. (**D**) Representative confocal microscopy images showing the area occupied by the microglial marker Iba1 at 3, 7 and 10 days. (**E**) Confocal microscopy projections showing DAPI-stained condensed nuclei. (**F**) Quantification of apoptotic cells in the slices at 3 , 7 and 10 days in the 4 different conditions. Scale bar is 10 μm. One-way ANOVA after all pair-wise multiple comparisons by Holm-Sidak post hoc test. Bars show mean ± SEM. Dots show individual data*$p < 0.05$, **$p < 0.01$, ***$p < 0.001$.

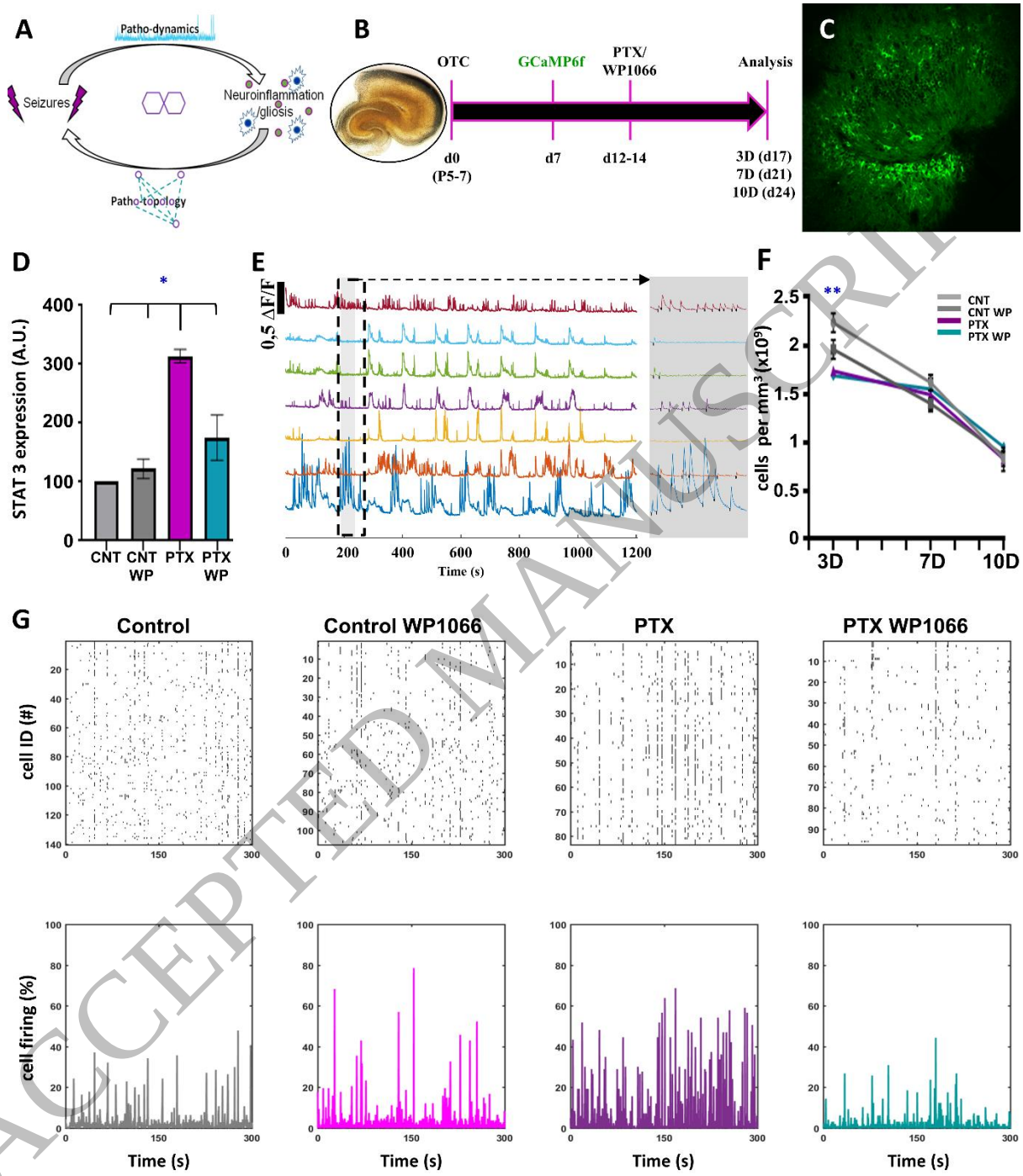

Figure 1
159x186 mm (x DPI)

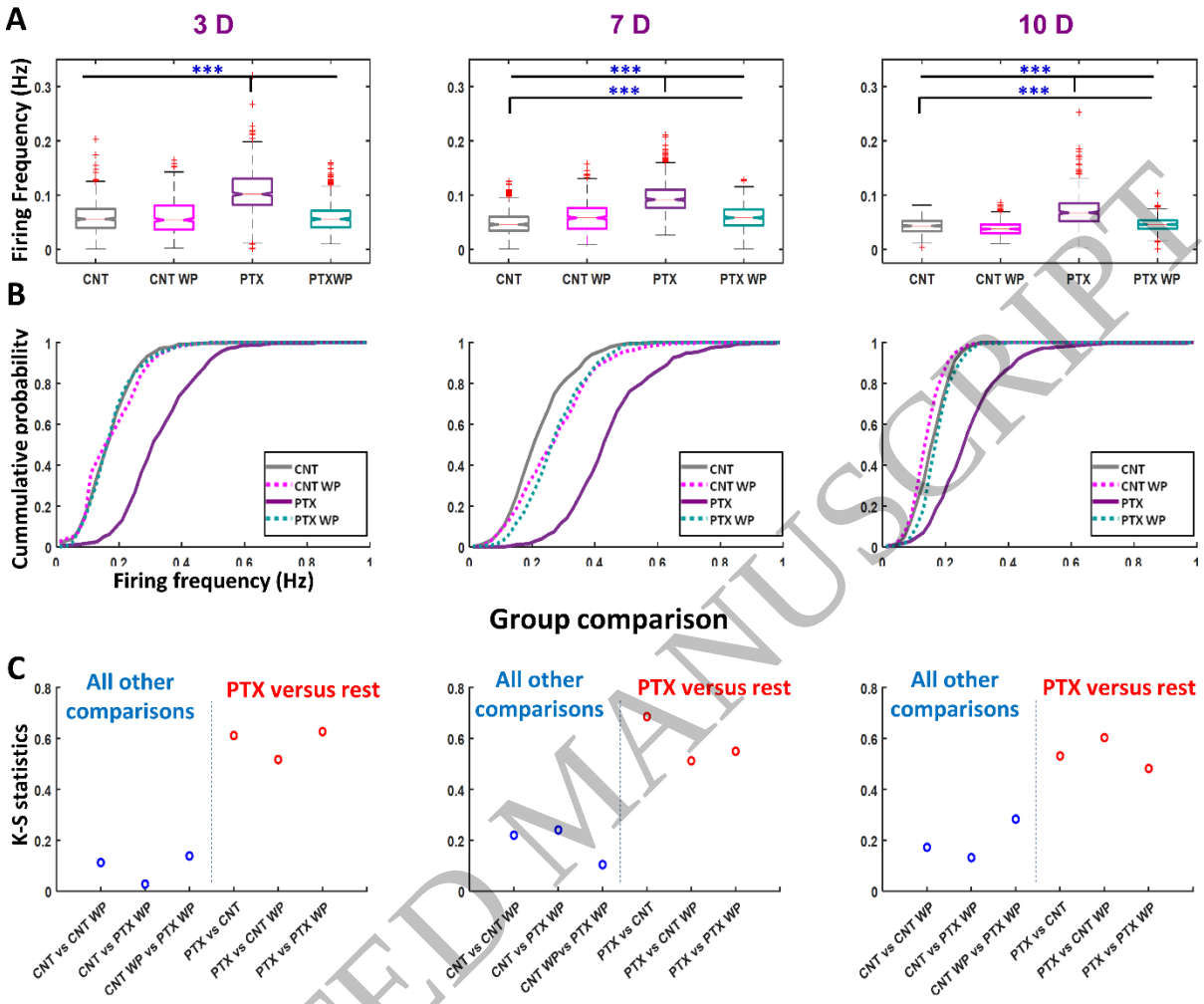

Figure 2
159x140 mm (x DPI)

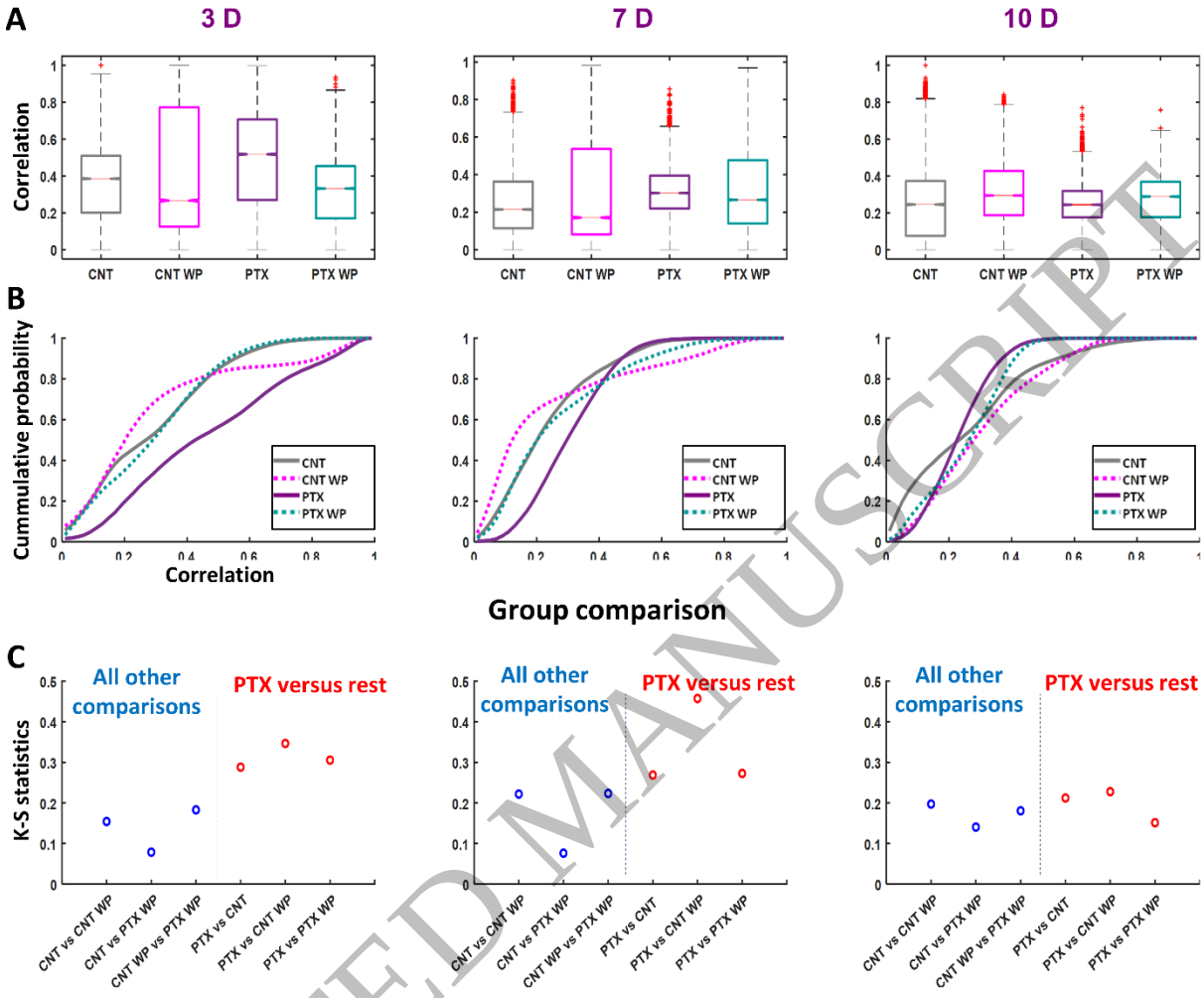

Figure 3
159x139 mm (x DPI)

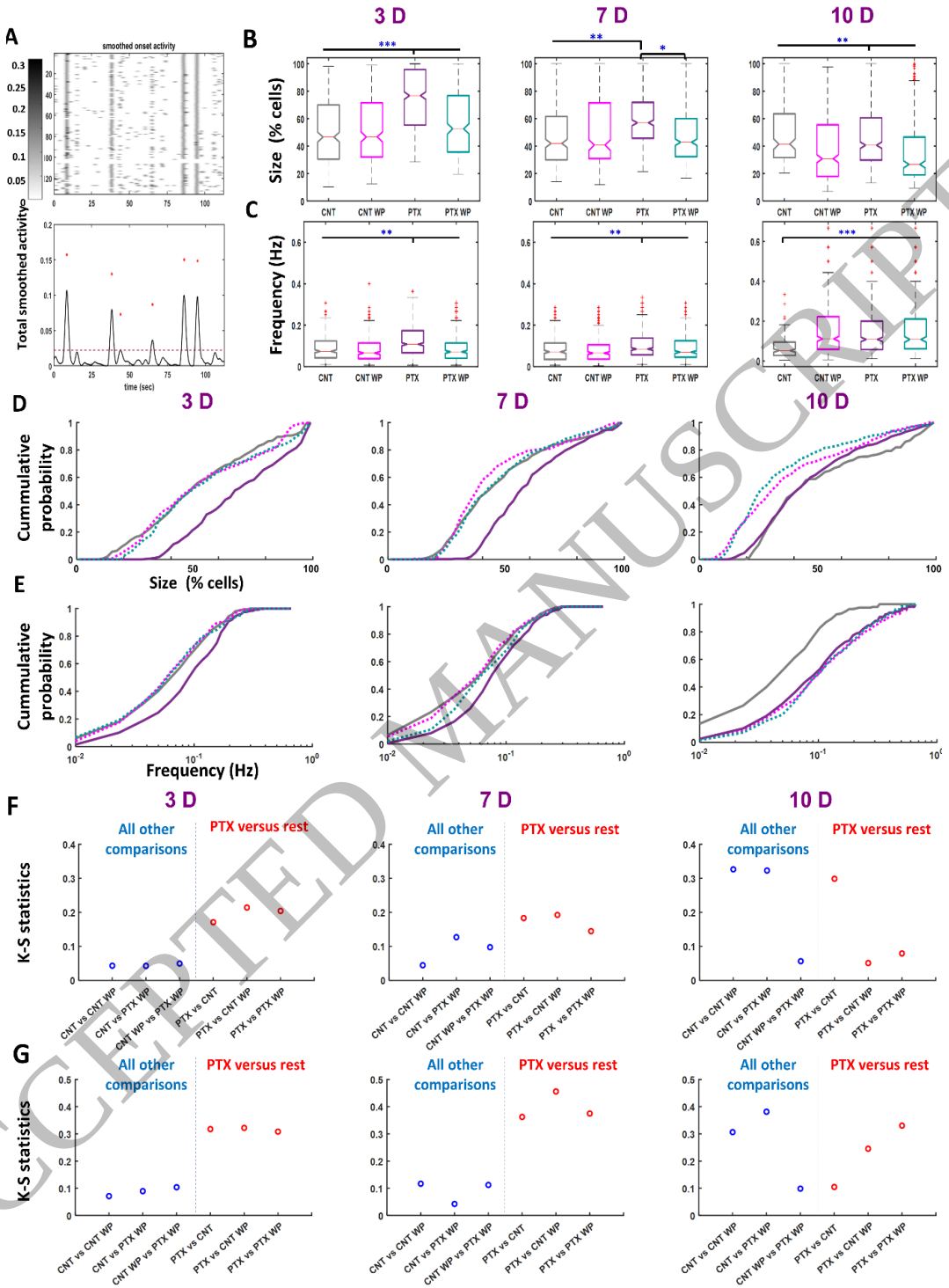

Figure 4
159x210 mm (x DPI)

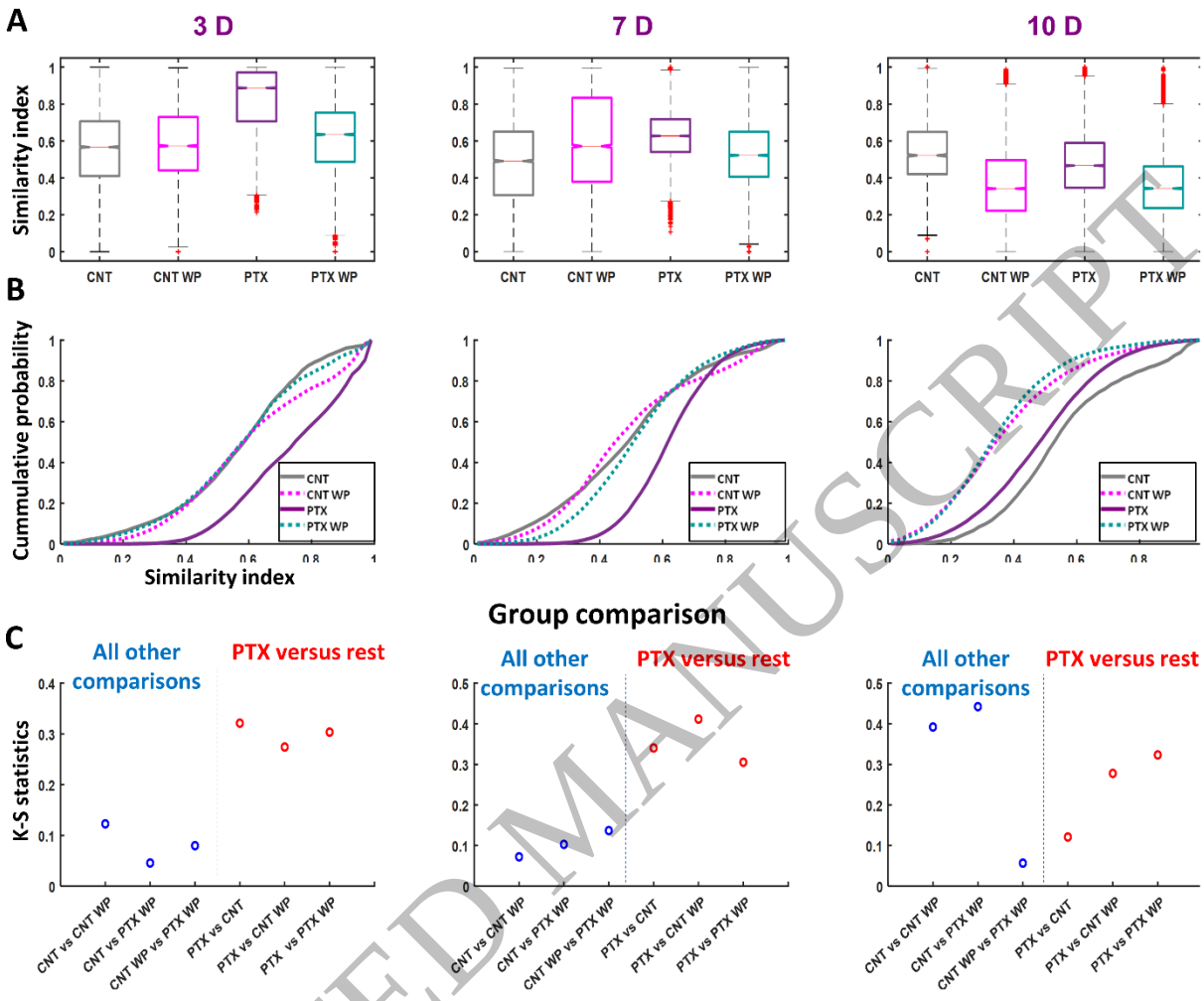

Figure 5
159x137 mm (x DPI)

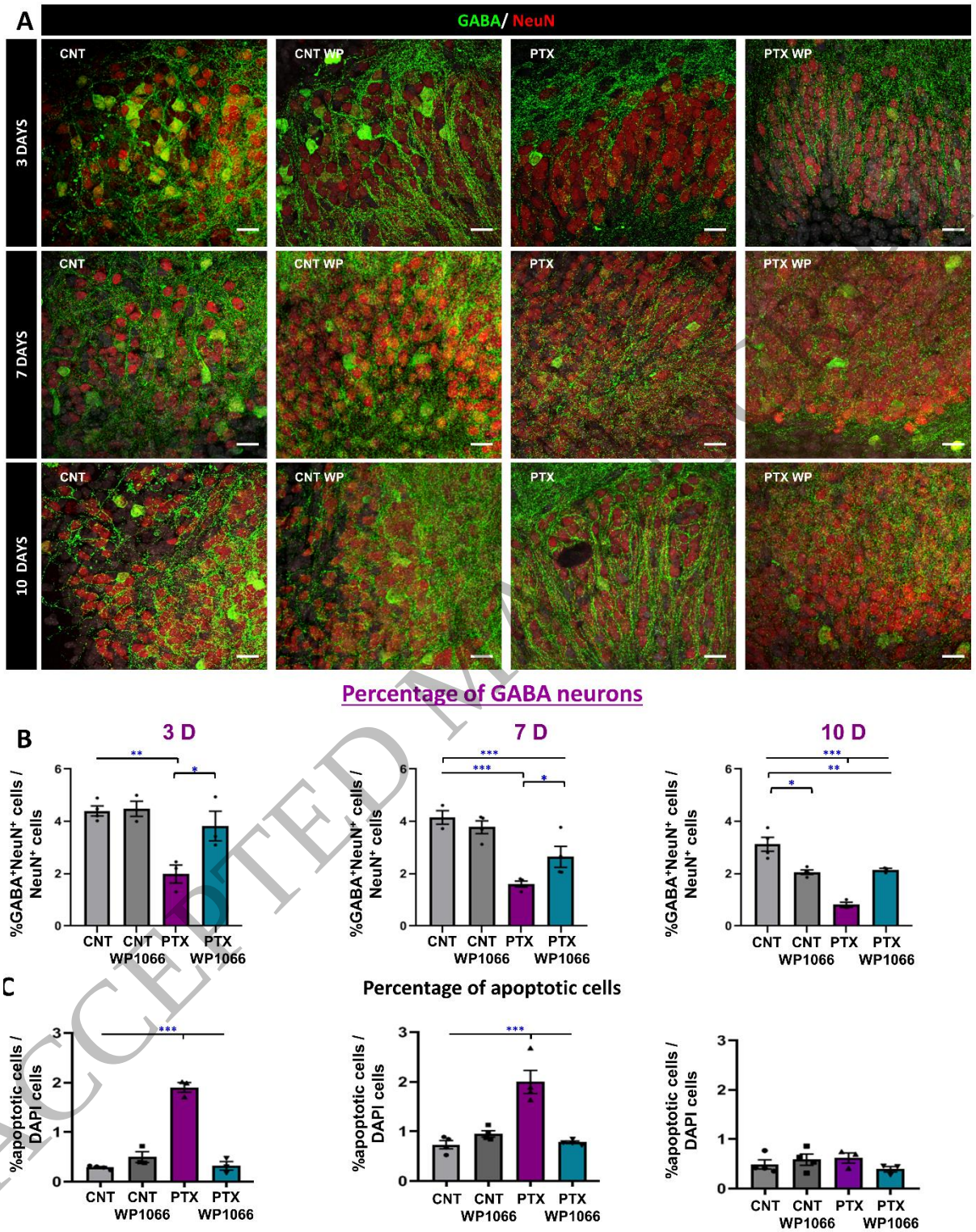

Figure 6
159x204 mm (x DPI)

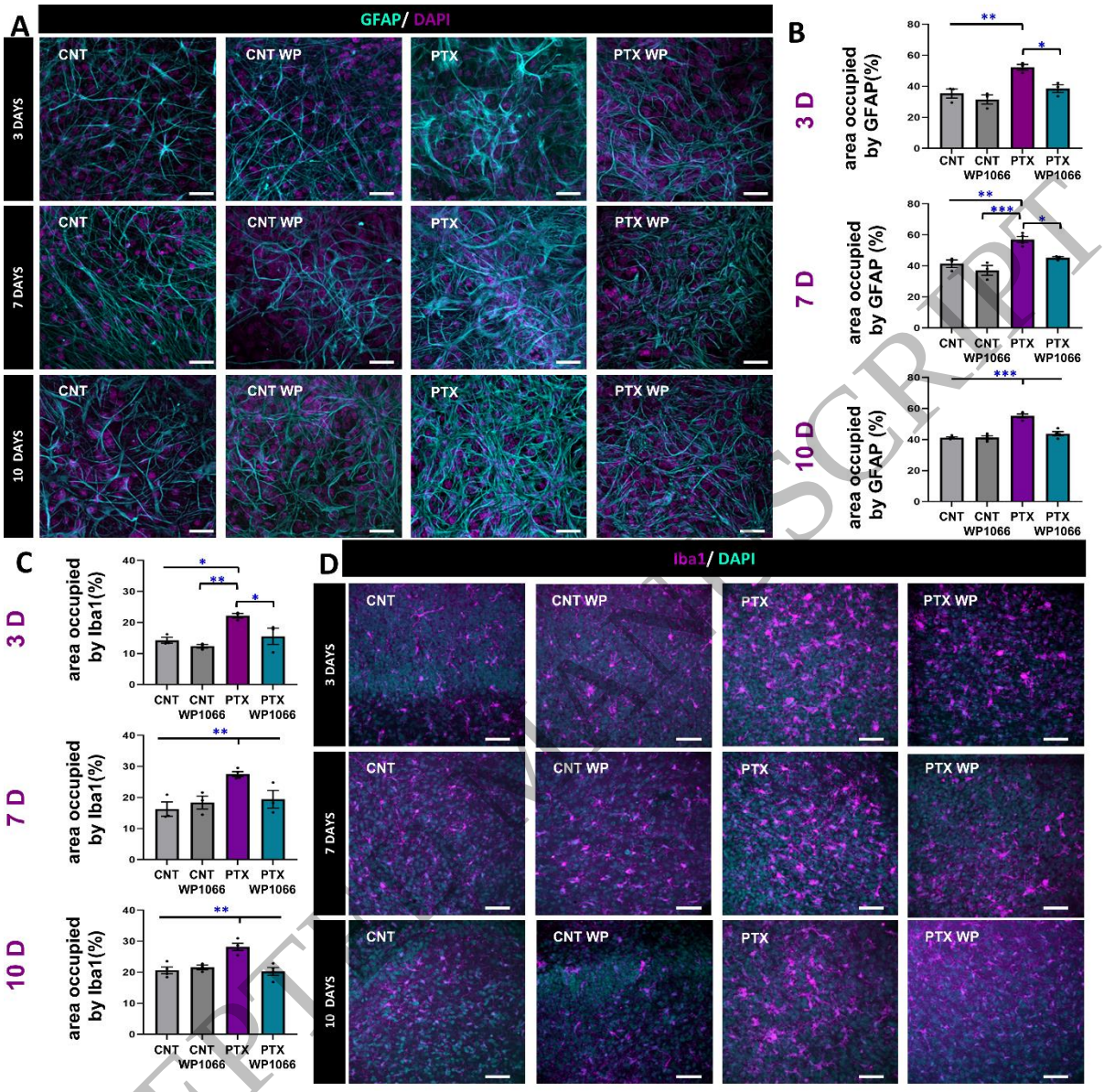

Figure 7
159x160 mm (x DPI)